Asian Journal of Chemistry; Vol. 29, No. 8 (2017), 1811-1816

ASIAN JOURNAL OF CHEMISTRY

https://doi.org/10.14233/ajchem.2017.20642

Structural, Dielectric and Electrical Properties of (1-x)$CaCu_3Ti_4O_{12}$–x$BaTiO_3$ Ceramics

N. HADI[1], T. LAMCHARFI[1,2], F. ABDI[1], N. GOUITAA[1], N.S. ECHATOUI[1] and M. ZOUHAIRI[2]

[1]Signals Systems and Components Laboratory, Faculte des Sciences et Techniques de Fes, Université Sidi Mohamed Ben Abdellah, Fez B.P. 2202, Morocco
[2]Chemistry Laboratory of Condensed Matter, Faculte des Sciences et Techniques de Fes, Université Sidi Mohamed Ben Abdellah, Fez B.P. 2202, Morocco

*Corresponding author: E-mail: zouhir963@gmail.com

Received: 10 March 2017; *Accepted*: 26 April 2017; *Published online*: 12 June 2017; AJC-18447

In this work, the effect of $BaTiO_3$ (BT) addition on structural, dielectric and electrical properties of $CaCu_3Ti_4O_{12}$ (CCTO) ceramic was investigated. Ceramic samples with the chemical formula (1-x)$CaCu_3Ti_4O_{12}$ – x$BaTiO_3$, (1-x)CCTO-xBT, (x = 0.00, 0.10, 0.20, 0.30, 0.50 and 1.00) were synthesized by solid state route. The structural studies carried out by X-ray diffraction technique and showed that the perovskite structure cubic and tetragonal phases were formed without any other impurity phases. The addition of $BaTiO_3$ into CCTO system lowered the last crystallite size to about 52 nm and increased the dielectric constant by four orders compared to pure CCTO. Moreover, the results of the complex impedance analyses of (1-x)CCTO–xBT ceramics samples confirmed the presence of non-Debye type of relaxation phenomenon and exhibited a negative temperature coefficient of resistance behaviour.

Keywords: Ceramics, Barium titanate, Raman spectroscopy.

INTRODUCTION

The materials which have a high dielectric constant attracted the attention of many researchers due to their use in many applications. Among those materials barium titanate ($BaTiO_3$) which belongs to a perovskite structure ABO_3 type [1-4]. The dielectric constant of these materials is highly unstable, vary with temperature and it is not suitable for using at high temperature. This reason attracts a lot of researches efforts to find a solution to solve this problem. The $CaCu_3Ti_4O_{12}$ (CCTO) ceramic is the results of these efforts and it was found that this material belongs to pseudo-cubic perovskite structure with the space group of Im3 and the lattice parameter of 7.391 Å [5-8] and has a high dielectric constant and thermal stability in the range of 100 to 400 K [1,9,10]. These have made perovskite a promising material in many applications in microelectronics. A high dielectric loss appeared in the CCTO ceramic process as compared with $BaTiO_3$ [1,6]. There are several researches on the CCTO and $BaTiO_3$ ceramics which tried to improve the dielectric properties of these materials by controlling the manufacturing operations such as method, substitution, sintering time or temperature and calcinations time or temperature [11-14] and others tried to identify the nature of continued high dielectric constant of these ceramics [15,16]. Through our knowledge there is no any work to manufacturing ceramic which follow a mixture CCTO and $BaTiO_3$ characteristics. In the present work we are reporting the synthesis of (1-x)CCTO–xBT by solid state reaction route. The structural, dielectric and electrical properties of (1-x)$CaCu_3Ti_4O_{12}$–x$BaTiO_3$ ceramics (where x = 0.00-1.00) were investigated.

EXPERIMENTAL

The (1-x)CCTO-(x)BT samples were synthesized by means of a conventional mixed oxide route. High-purity oxides and carbonates; $CaCO_3$ (99.8 %) CuO (purity, 99 %), TiO_2 (purity, 99.95 %) and $BaCO_3$ (purity 99.5 %) (All Sigma Aldrich chemicals, USA) were used as starting materials.

Synthesis of (1-x)$CaCu_3Ti_4O_{12}$–x$BaTiO_3$: The powders were weighed in stoichiometric proportion and milled for 1 h. Then the slurry was dried in an oven at 80 °C. The calcinations processes of CCTO and $BaTiO_3$ powders were carried at 1050 °C and 1100 °C for 4 h, respectively. The synthesized powders were mixed in acetone according to the formula (1-x)CCTO-(x)BT for 2 h and dried at 400 °C for 1 h, after that the powders were crushed in agate mortar and pressed into pellets of about 12 mm diameter and 1.5 mm thickness. Then, the pellets sintered at 1050 °C for 8 h and left at room temperature. The samples surfaces were coated by silver paste to serve as poles for the electrical measurements uses.

Characterization of (1-x)$CaCu_3Ti_4O_{12}$–x$BaTiO_3$

XRD analysis: The crystal structure of (1-x)CCTO-xBT was determined by using an X-ray diffractometer with a scanning rate of 0.02°/min for 2θ range 20°-80° by employing CuK_α radiation wavelength λ = 1.5406 Å (diffractometer system = XPERT-PRO) under the conditions of 40 KV and 30 mA.

Raman spectroscopy analysis: A micro Raman spectrometer, equipped with an excitation source of monochromatic with wavelength of 410 nm, was used to study the relationship between Raman lines and different types of atomic motions of CCTO and $BaTiO_3$ in the (1-x)CCTO-xBT ceramics. After the sample processing, Raman spectra was collected at room temperature.

Dielectric measurements analysis: The electrical properties of the ceramics were measured as a function of frequency (100 Hz - 2 MHz) and temperature (room temperature (RT) - 220 °C) by using an impedance analyzer.

RESULTS AND DISCUSSION

X-ray diffraction analysis: Fig. 1 shows the XRD patterns of (1-x)CCTO–(x)BT ceramics. All the diffraction peaks were indexed to a cubic perovskite structure with Im3 space group for x = 0 (CCTO) sample and a tetragonal phase for x = 1 (pure $BaTiO_3$). While the X-ray analysis for (1-x)CCTO–xBT at 80 ≥ x ≥ 10 showed the coexistence of cubic and tetragonal phases without any other impurity phases (Fig. 1a). However, the XRD patterns show the presence of split in the (220) peak of all the samples except at x = 0.1 sample (Fig. 1b), this difference may be has a role in change of the structural proprieties. It is noted that the distinctive peak of CCTO (220) shifted to the high degrees with the increase of $BaTiO_3$ addition. The lattice parameter of undoped CCTO (x = 0) sample is 0.7391 nm which is the same value reported by previous workers [1,5,8]. However, for $BaTiO_3$ doping the lattice parameter of CCTO ceramic decreases from 0.7391 to 0.7385 nm as reported in Table-1, leading to the shift of (220) peaks of CCTO ceramics towards larger angles indicating a slight reaction in the mixture during the preparation process according to the interpretation reported in the literature [17]. These results show that the $BaTiO_3$ addition does not change the pseudo-cubic perovskite structure of CCTO, but change in the $BaTiO_3$ structure from tetragonal at x = 1.00 to pseudo-cubic at x = 0.10 (Table-1). The average crystallite size of the CCTO and $BaTiO_3$ in (1-x)CCTO–xBT was estimated from the X-ray line broadening of the (220) and (101) peak, respectively by using the Scherrer formula [17]:

$$D = \frac{0.9\lambda}{\beta\cos\theta} \quad (1)$$

where D is the average particle size, λ is the wavelength of used X-rays and β is the full width of the diffraction peak (FWHM) at half-maximum for the diffraction angle 2θ. The parameter β was corrected for instrumental width using the following equation:

$$\beta = \sqrt{\beta_{exp}^{\ 2} - \beta_{inst}^{\ 2}} \quad (2)$$

where β_{exp} is the experimental width and β_{inst} instrumental width that are extracted from a sample pattern of LaB_6 [3,17-19]. For this purpose, we chose the single peaks near 34° and 31° within the pattern and according to the space group of CCTO and $BaTiO_3$, respectively. The particle size values of CCTO and $BaTiO_3$ are given in Table-1. It is noticed that the CCTO crystallite size decreases with 22 % rate with the increase of $BaTiO_3$ content, while the $BaTiO_3$ crystallite size shows an increase with 4 % rate. The values of particle size obtained in this study for CCTO and $BaTiO_3$ were in good agreement with those mentioned in the literature [4,20-22].

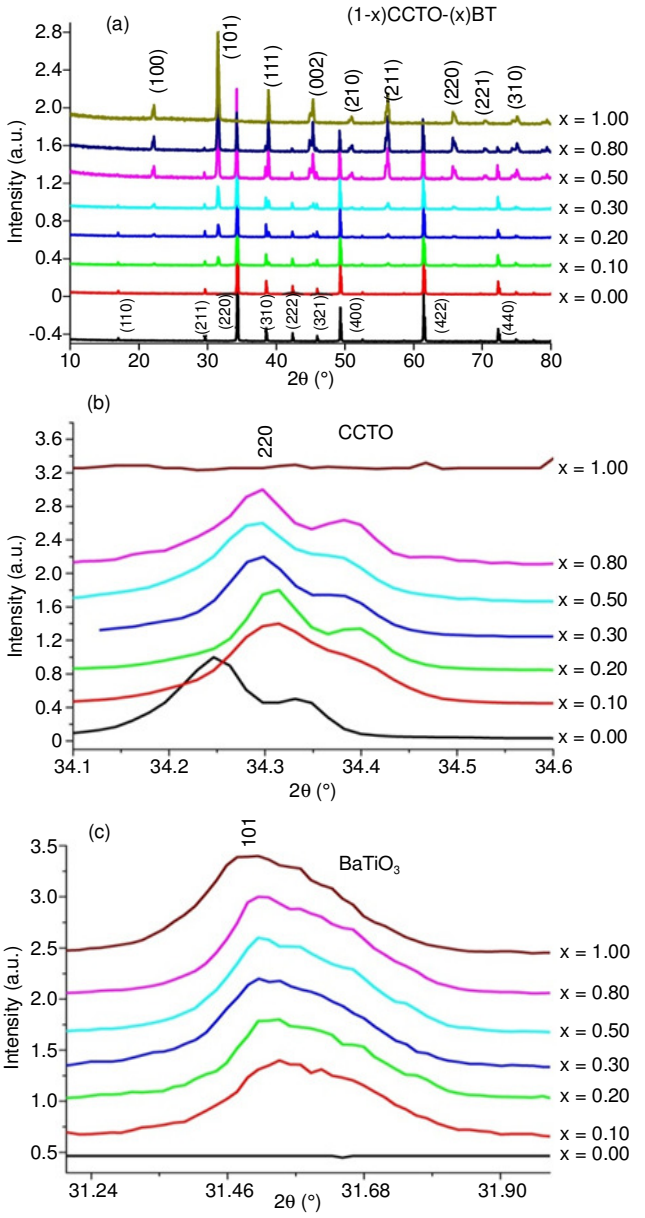

Fig. 1. (a) XRD of $BaTiO_3$ doped CCTO ceramics (b and c) enlarged XRD patterns of the ceramics for 2θ = 34° and 31°, respectively, for all compositions

Raman spectroscopy analysis: Fig. 2 represents the Raman spectra of CCTO, $BaTiO_3$ and (1-x)$CaCu_3Ti_4O_{12}$ –x$BaTiO_3$ ceramics. Six main peaks of Raman modes at 288, 405, 448, 509, 579 and 745 cm^{-1} were observed for pure CCTO sample as shown in Fig. 2. These peaks are compared with the theoretical values from the lattice dynamics calculations (LDC) by Kolev *et al.* [24-26] and with the experimental values as shown in Table-2. The LDC calculations have predicted eight peaks

TABLE-1
SYSTEM, LATTICE PARAMETERS AND CRYSTALLITE SIZE OF CCTO AND BT IN (1-x)CCTO–xBT COMPOSITION OBTAINED FROM THE X-RAY DIFFRACTION

Composition x	System CCTO	System BT	Lattice parameter "a" CCTO	Lattice parameter "a" BT	Lattice parameter "c" BT	Crystallite size (nm) CCTO	Crystallite size (nm) BT
0.00	Cubic	–	0.7391	–	–	67.756	–
0.10	Cubic	Cubic	0.7388	0.3965	0.3965	56.198	29.983
0.20	Cubic	Tetragonal	0.7389	0.3995	0.4031	65.187	31.329
0.30	Cubic	Tetragonal	0.7388	0.4036	0.4005	63.466	30.416
0.50	Cubic	Tetragonal	0.7385	0.3994	0.4030	56.348	30.580
0.80	Cubic	Tetragonal	0.7393	0.3993	0.4038	52.997	30.518
1.00	–	Tetragonal	–	0.3993	0.4100	–	30.929

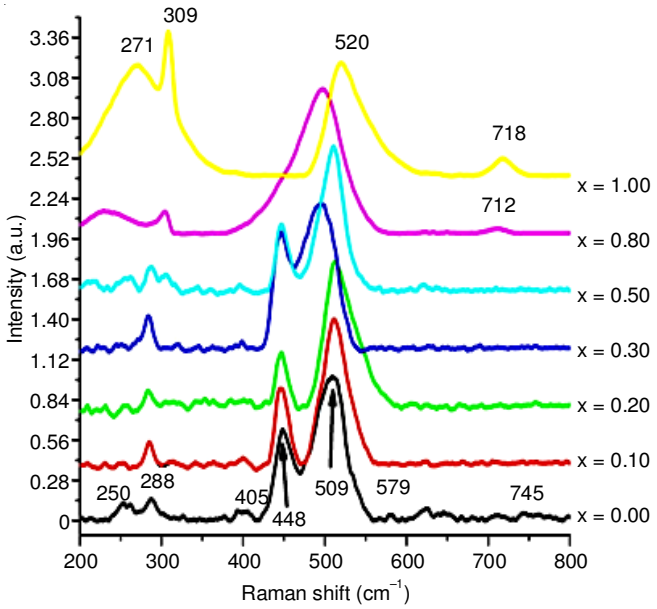

Fig. 2. Raman spectra of (1-x)CCTO-xBT powders

in Raman spectrum representing different vibration mode in CCTO. According to the Table-2, the peak position of the Raman spectra of present sample are in a good agreement with six over locations predicted by LDC. The peak noted at 250 cm^{-1} is due to the presence of copper oxide and it is not explicit in the X-ray diffraction measurements [25].

The Raman spectrum of the $BaTiO_3$ powder shows four main peaks at 271, 309, 520 and 718 cm^{-1} (Table-2) in a frequency range from 200 to 800 cm^{-1}. The wide peak at 271 cm^{-1} is attributed to the A_1(LO) mode. The band at 718 cm^{-1} is associated with the highest frequency LO mode of A_1 symmetry. The sharp peak located at 309 cm^{-1} is associated to the E(TO+LO) mode and present the characteristic peak of tetragonal $BaTiO_3$ phase. The peak observed at 520 cm^{-1} is assigned to the A1(TO) mode. The Raman modes of the pure sample $BaTiO_3$ are in good agreement with the values reported in the literature [22] and tabulated in Table-2. The peaks obtained for pure $BaTiO_3$ and CCTO samples were also observed for $CaCu_3Ti_4O_{12}$-$BaTiO_3$ ceramics, those peaks were observed separately at low concentrations of $BaTiO_3$ in CCTO (x = 0.10, 0.20 and 0.30). With the increase of $BaTiO_3$ addition, the Raman spectrum revealed the overlapping of the $BaTiO_3$ and CCTO peaks. For (0.50 CCTO - 0.50 $BaTiO_3$) composite ceramic we can easily identify all the modes associated to the CCTO and $BaTiO_3$ at 262, 288, 308, 459 and 511 cm^{-1}, while the modes associated to the CCTO at 448 and 509 cm^{-1} in (0,80 CCTO - 0,20 $BaTiO_3$) composite are overlapped with the band at 520 cm^{-1} associated to the $BaTiO_3$ ceramic, accompanied with the shift of this peak to the low-frequency region, whereas the peaks at 401 and 579 cm^{-1} were not detected. We note also that the peak at 250 cm^{-1} disappears at x = 0.10 sample and appears again at x = 0.20 and 0.50. The vibration modes are affected by the fluctuations caused by the phase change, especially the intensity of the peak at 309 cm^{-1} assigned to the modes E(Ti-O), which disappears in the samples (x = 0.10-0.30). This may be due to the phase transition.

Dielectric properties: The real part of the complex permitivity of the dielectric constant ($\varepsilon_{r'}$), at the various temperatures is calculated by using the measured capacitance values (C_p) according to the following relation:

$$\varepsilon_{r'} = C_p d/\varepsilon_o S \quad (3)$$

where ε_o is the dielectric constant of free space, d is the thickness and S is the area of the disk. The variation of dielectric

TABLE-2
RAMAN MODES OF THE (1-x) CCTO-xBT CERAMICS (x = 0.00-1.00)

Modes	$BaTiO_3$ [Ref. 22]	LDC [Ref. 24]	CCTO [Ref. 22]	x = 0.00 $BaTiO_3$ (CCTO)	x = 1.00 $BaTiO_3$	x = 0.20 $BaTiO_3$	x = 0.30 $BaTiO_3$	x = 0.50 $BaTiO_3$	x = 0.80 $BaTiO_3$
A_1 (O–Ti–O)	264	–			271		265	262	230
E (Ti–O)	307	–			309		305	308	304
A_1 (Ti–O)	519	–			520				498
A_1 (TiO_6)	718	–			712				712
Ag(1)	–	428	443	448		447	447	459	
Ag(2)	–	512	505	509		513	496	511	
Eg(1)	–	318					320		318
Eg(2)	–	548							
Fg(1)	–	280	283	288		283	288	288	
Fg(2)	–	405		405			398		
Fg(3)	–	574	571	579					
Fg(4)	–	747	747	745					

constant for CCTO, $BaTiO_3$ and (1-x)CCTO-xBT ceramics (x = 0.00 –1.00) in a wide frequency range (1 kHz to 2 MHz) at room temperature and different temperatures is given in Fig. 3. It is noticed that the CCTO ceramic presents a higher ε_r compared to $BaTiO_3$ in the range of frequencies of 1 kHz to 1MHZ then the opposite happened at high frequencies above 1 MHz (Fig. 3). At 1 kHz the value is around 6285 for the CCTO ceramic compared to 900 for the $BaTiO_3$ ceramic (Fig. 3a,f and Table-3). However for the composites (1-x)CCTO-xBT) ceramics at x = 0.10-0.40 have an unexpected results. The values of ε_r are $6285 < \varepsilon_r \leq 26715$, which is more than four times higher compared to the CCTO value (Fig. 3a-c). The present results are consistent with the results reported in the literature [22]. While at high concentrations ($x \geq 0.5$) the ε_r values are $980 < \varepsilon_r \leq 6285$, which are four times less than the CCTO value (Fig. 3d-e). Our results at high concentrations were approach with the results obtained by the Norezan *et al.* [27]. As it is observed also from Fig. 3 (Table-3) that the dielectric constant of samples x = 0.00-0.30 declines slightly in the frequency region below 1 MHz, following by a dramatic decrease of dielectric constant above 1 MHz, but the samples at high concentrations ($x \geq 0.50$) showed rapidly decreases in ε_r values with increasing a frequency as compared with CCTO, $BaTiO_3$ and (1-x)CCTO-xBT at low concentrations. The decrease of dielectric constant with increasing frequency is attributed to the interfacial polarization, which occurs due to decrease in the accumulation of charge carriers at the interface of semiconducting grain and insulating grain boundary [28]. However, in the higher frequency region of f > 1 MHz (Fig. 3a-f), the dielectric constant of samples $x \geq 0.50$ are higher than that samples at concentration range of x = 0.00-0.40. So, it can be suggested that addition of $BaTiO_3$ to CCTO more than 0.50 played a role in strengthening the dielectric constant at high frequencies. On the other hand, the ε_r value increases with rise of temperature. This increase can be explained on the basis of the ability of dipoles to align orientation. Furthermore, at higher temperature the accumulation of charge carrier increases at the interface between grain and grain boundary [24].

Electric properties: Dielectric relaxation phenomenon is usually performed by measurements in the frequency region and the data can be represented on the complex impedance plane by using the Cole-Cole function. Fig. 4(a-e) show the complex impedance spectrum Z″ as function of Z′ of (1-x)CCTO-xBT (x = 0.10, 0.20, 0.50 and 0.80) ceramics at different temperatures. The effect of $BaTiO_3$ concentration and temperature on impedance and related parameters of ceramics become easily observed with the increase in $BaTiO_3$ addition or a rise temperature. However, with the increase of $BaTiO_3$ content, the slope of the curve decreases towards of real axis and finally forms semicircles. The same effect can be observed with arise measu-

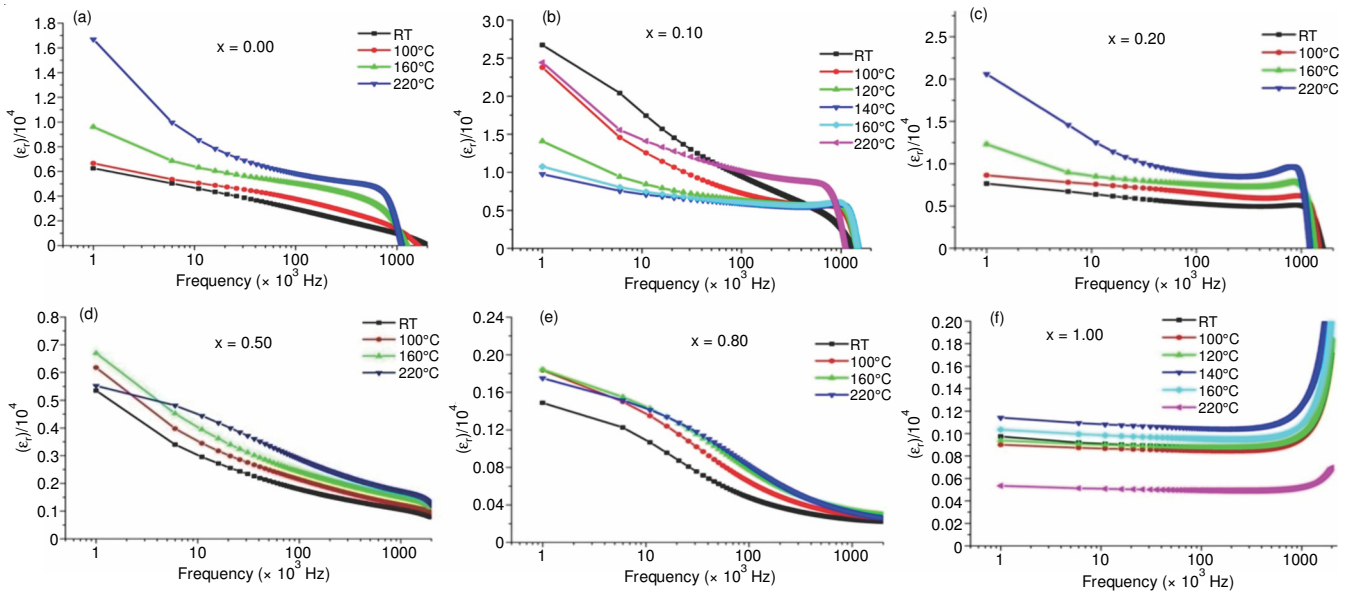

Fig. 3. Dielectric constant variation as function of frequency at different temperatures for (1-x)CCTO-xBT ceramics

TABLE-3
DIELECTRIC CONSTANT AT DIFFERENT TEMPERATURES AND FREQUENCIES

Composition	ε_r					
x =	RT at 1 kHz/1 MHz	100 °C 1 kHz/1 MHz	120 °C 1 kHz/1 MHz	140 °C 1 kHz/1 MHz	160 °C 1 kHz/1 MHz	220 °C 1 kHz/1 MHz
0.00	6285, 986	6663, 1338	7591, 1430	8617, 1514	9600, 1646	16690, 1506
0.10	26715, 2547	23765, 5116	14073, 5707	9762, 5879	10763, 5997	18507, 4971
0.20	7658, 505	8507, 5960	9385, 6487	10067, 6916	12295, 7496	20596, 8147
0.30	22764, 8118	12857, 7963	19392, 8167	19187, 8416	19125, 8600	22972, 11553
0.40	16949, 252	9083, 1115	8003, 1663	7405, 2905	7705, 3603	11583, 5225
0.50	4702, 1027	6177, 1230	6455, 1315	6493, 1398	6695, 1485	5519, 1726
0.80	1882, 267	1835, 290	1859, 303	1820, 319	1840, 337	1750, 324
1.00	900, 980	901, 955	939, 994	1141, 1233	1035, 1076	534, 523

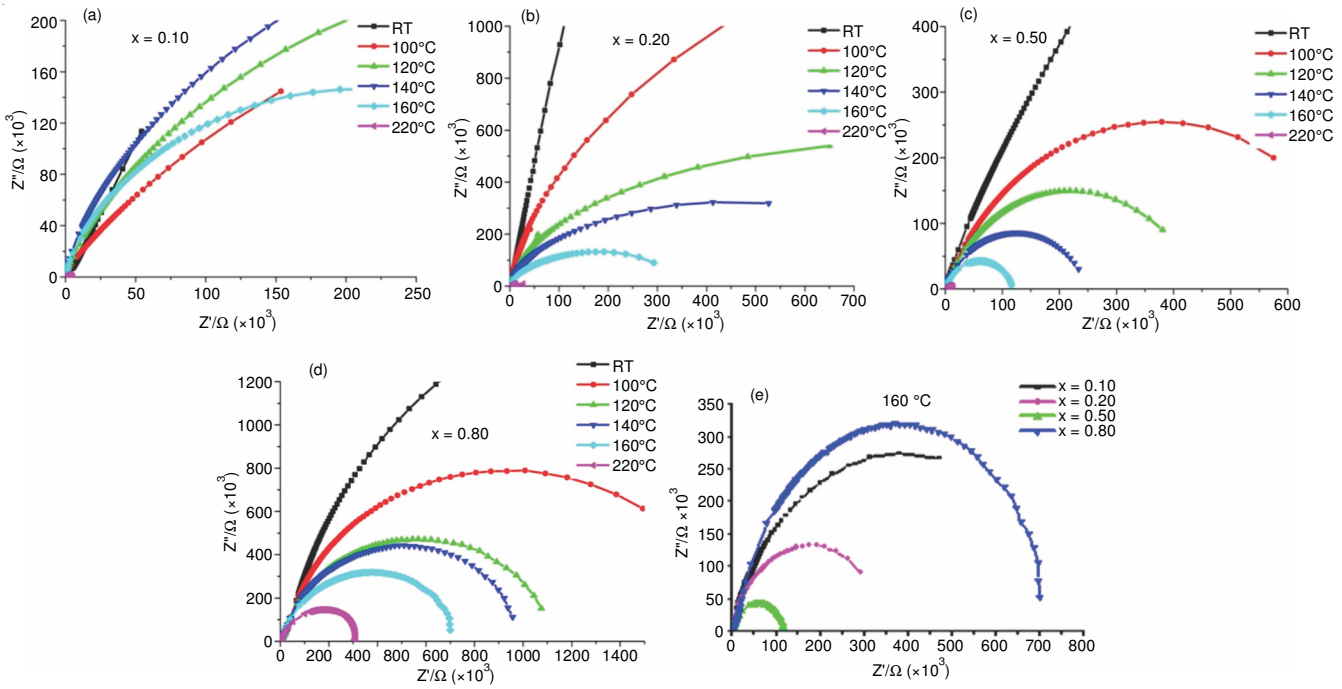

Fig. 4. Variation of real and imaginary part of impedance with temperature of (1-x)CCTO-xBT ceramic at a) x = 0.10, b) x = 0.20, c) x = 0.50, d) x = 0.80 and e) compared between them at 160 °C

rement temperature for each sample (Fig. 4a-d). In the figure, only one semicircle is clearly observed for all ceramics. This arc arise mainly due to the contribution of grain effects in each sample [23,28,29]. The arc has centers lying below the Z' axis related to the distribution of relaxation time, this behaviour confirming the presence of non-idial or non-Debye type of relaxation phenomenon in the ceramics [23,30]. The resistances corresponding to grain (R_g) and grain boundary (R_{gb}) are obtained from the intercepts of Z'-axis at higher and lower frequency, respectively [31]. These results showed that the resistance of grain and grain-boundary decrease with increasing in temperature for all samples. It suggests that the ceramic samples showed that the negative temperature coefficient of resistance (NTCR) type behaviour. The same behaviour can be observed with the increase in the $BaTiO_3$ concentration to 0.50 at each temperature for example at 160 °C (Fig. 4e).

Conclusion

In the present work, we have prepared (1-x)CCTO-xBT system with compositions of x = 0.00-1.00 by using solid state reaction route. X-ray diffraction pattern shows the formation of a pure phase for x = 0.00 and 1.00 composition and a composite phases for x = 0.10-0.80 compositions. The Raman spectra in case of pure of $BaTiO_3$ and CCTO powder showed the presence of four and six main peaks, respectively. while for (1-x)CCTO-xBT composite ceramics mode associated to the $BaTiO_3$ ceramic at low concentration (x = 0.10-0.30) are not detected, but those associated to the CCTO were observed. The dielectric study shows that for low concentration (x = 0.10-0.30), an increase of dielectric constant value by four orders was found, while above this concentration a decrease in dielectric constant values was observed, as compared to pure CCTO. The impedance analysis confirms the presence of non-Debye type relaxation phenomenon in the ceramics. They also support the typical behaviour of negative temperature coefficient of resistance.

REFERENCES

1 L. Singh, S.U. Rai, K.D. Mandal, B.C. Sin, H. Lee, H. Chung and Y. Lee, *Mater. Charact.*, **96**, 54 (2014); https://doi.org/10.1016/j.matchar.2014.07.019.

2. A. Chamola, H. Singh and U. C. Naithani, *Adv. Mater. Lett.*, **2**, 148 (2011); https://doi.org/10.5185/amlett.2010.11183.

3. A.F.L. Almeida, P.B.A. Fechine, M.P.F. Graça, M.A. Valente and A.S.B. Sombra, *J. Mater. Sci. Mater. Electron.*, **20**, 163 (2009); https://doi.org/10.1007/s10854-008-9675-4.

4. P. Fiorenza, V. Raineri, S.G. Ebbinghaus and R.L. Nigro, *CrystEngComm*, **13**, 3900 (2011); https://doi.org/10.1039/C0CE00948B.

5. L. Singh, U.S. Rai, K.D. Mandal and N.B. Singh, *Prog. Cryst. Growth Charact. Mater.*, **60**, 15 (2014); https://doi.org/10.1016/j.pcrysgrow.2014.04.001.

6. V.S. Saji and H.C. Choe, *Thin Solid Films*, **517**, 3896 (2009); https://doi.org/10.1016/j.tsf.2009.01.100.

7. Ajay Pratap Singh. et al., 3, 247 (2014) (Name of the Journal missing)

8. S. Jesurani, S. Kanagesan, R. Velmurugan and T. Kalaivani, *Trans. Indian Ceram. Soc.*, **70**, 79 (2011); https://doi.org/10.1080/0371750X.2011.10600152.

9. S.A. Ellyawan, Ph.D. Thesis, Bulk and Grain Boundary Electrical Behaviours in Nb and Sn Doped Calcium Copper Titanium Oxide, University of Manchester, UK (2014).

10. J. Liu, R.W. Smith and W.-N. Mei, *Chem. Mater.*, **19**, 6020 (2007); https://doi.org/10.1021/cm0716553.

11. T. Badapanda, R. Harichandan, S. Nayak, A. Mishra and S. Anwar, *Process. Appl. Ceram.*, **8**, 145 (2014); https://doi.org/10.2298/PAC1403145B.

12. W. Li and R.W. Schwartz, *Appl. Phys. Lett.*, **89**, 242906 (2006); https://doi.org/10.1063/1.2405382.

13. P.R. Bueno, W.C. Ribeiro, M.A. Ramírez, J.A. Varela and E. Longo, *Appl. Phys. Lett.*, **90**, 142912 (2007); https://doi.org/10.1063/1.2720301.

14. R. Schmidt, C.M. Stennett, C.N. Hyatt, J. Pokorny, J. Prado-Gonjal, M. Li and C.D. Sinclair, *J. Eur. Ceram. Soc.*, **32**, 3313 (2012); https://doi.org/10.1016/j.jeurceramsoc.2012.03.040.

15. A. Tselev, M.C. Brooks, M.S. Anlage, H. Zheng, L. Salamanca-Riba, R. Ramesh and M.A. Subramanian, *Phys. Rev. B*, **70**, 144101 (2004); https://doi.org/10.1103/PhysRevB.70.144101.

16. B. Barbier, C. Combettes, S. Guillemet-Fritsch, T. Chartier, F. Rossignol, A. Rumeau, T. Lebey and E. Dutarde, *J. Eur. Ceram. Soc*., **29**, 731 (2009); https://doi.org/10.1016/j.jeurceramsoc.2008.07.042.
17. V. Senthil, T. Badapanda, A.B. Chandra and S. Panigrahi, *ISRN Ceramics*, **Article ID 943734** (2012); https://doi.org/10.5402/2012/943734.
18. S. Suresh, *Int. J. Phys. Sci.*, **8**, 1121 (2013); https://doi.org/10.5897/IJPS2013.3926.
19. T. Badapanda, S. Venkatesan, S. Panigrahi and P. Kumar, *Process. Appl. Ceramics*, **7**, 135 (2013); https://doi.org/10.2298/PAC1303135B.
20. B. Mohanty, P.S. Sahoo, M.P.K. Sahoo and R.N.P. Choudhary, *J. Mod. Phys.*, **3**, 357 (2012); https://doi.org/10.4236/jmp.2012.35050.
21. S.K. Rao and M.D. Prasad, *Ceram. Silik.*, **52**, 190 (2008).
22. A.F.L. Almeida, P.B.A. Fechine, J.C. Góes, M.A. Valente, M.A.R. Miranda and A.S.B. Sombra, *Mater. Sci. Eng. B*, **111**, 113 (2004); https://doi.org/10.1016/j.mseb.2004.03.027.
23. R. Kumar, R. Rani and S. Sharma, *Adv. Mater. Lett.*, **5**, 658 (2014); https://doi.org/10.5185/amlett.2014.3600.
24. N. Kolev, R.P. Bontchev, M.A.J. Jacobson, V.N. Popov, V.G. Hadjiev, A.P. Litvinchuk and M.N. Iliev, *Phys. Rev. B*, **66**, 132102 (2002); https://doi.org/10.1103/PhysRevB.66.132102.
25. J. Liu, R.W. Smith and W.-N. Mei, *Chem. Mater*., 19, 6020 (2007); https://doi.org/10.1021/cm0716553.
26. C. Mingxiang, P.H.D. Thesis, Extrinsic Dielectric Relaxation of Colossal Dielectric Constant Material $CaCu_3Ti_4O_{12}$, Department of Applied Physics, Polytechnic University, Hong Kong (2011).
27. I. Norezan, A.K. Yahya and M.K. Talari, *J. Mater. Sci. Technol.*, **28**, 1137 (2012); https://doi.org/10.1016/S1005-0302(12)60183-2.
28. L. Singh, U.S. Rai, K.D. Mandal and A.K. Rai, *Appl. Phys. A*, **112**, 891 (2013); https://doi.org/10.1007/s00339(2012)012-7443-z.
29. E.J.J. Mallmann, M.A.S. Silva, A.S.B. Sombra, M.A. Botelho, S.E. Mazzetto, A.S. de Menezes, A.F.L. Almeida and P.B.A. Fechine, J. Electr. Mater., **44**, 295 (2015); https://doi.org/10.1007/s11664-014-3464-z.
30. J. Shanker, M.B. Suresh and D.S. Babu, *Int. J. Sci. Eng. Res.*, **3**, 194 (2015).
31. L. Singh, K.D. Mandal, U.S. Rai and A.K. Rai, *Indian J. Phys.*, **88**, 665 (2014); https://doi.org/10.1007/s12648-014-0471-0.